Nano Energy 64 (2019) 103904

Contents lists available at ScienceDirect

Nano Energy

journal homepage: www.elsevier.com/locate/nanoen

Full paper

# Transparent and stretchable bimodal triboelectric nanogenerators with hierarchical micro-nanostructures for mechanical and water energy harvesting

Xiaoliang Chen[a], Jiaqing Xiong[b], Kaushik Parida[b,d], Meiling Guo[c], Cheng Wang[c], Chao Wang[a], Xiangming Li[a], Jinyou Shao[a,*], Pooi See Lee[b,d,**]

[a] State Key Laboratory for Manufacturing Systems Engineering, Xi'an Jiaotong University, Xi'an, Shaanxi, 710049, China
[b] School of Materials Science and Engineering, Nanyang Technological University, 50 Nanyang Avenue, 639798, Singapore
[c] School of Mechanical and Precision Instrument Engineering, Xi'an University of Technology, Xi'an, 710048, China
[d] Singapore-HUJ Alliance for Research and Enterprise (SHARE), Nanomaterials for Energy and Energy Water Nexus, (NEW), Campus for Research Excellence and Technological Enterprise (CREATE), 138602, Singapore

ARTICLE INFO

*Keywords:*
Nanogenerator
Hierarchical structure
Bimodal
Stretchable
Water energy

ABSTRACT

Advances in flexible electronics set new requirements of highly deformable energy generators to power these electronic devices. It is still a challenge to simultaneously achieve high stretchability and strong power generation for most energy generators to adapt the practical flexible applications. Herein, a hierarchical micro-nanostructure featured with high transparency, full stretchability, and superhydrophobicity is first created to construct high performance bimodal triboelectric nanogenerators (TENGs) for harvesting mechanical energy and water energy. The core $SiO_2$/poly[vinylidenelfuoride-co-trifluoroethylene) P(VDF-TrFE) hierarchical micro-nanostructure is fabricated by a scalable electrospinning technology, and then reliably transferred to a pre-stretched elastomer to achieve robust stretchability and superhydrophobicity. Owing to the significantly increased surface roughness, the triboelectric output of the hierarchical structure is enhanced by 3 times higher than that of the pristine bulk film. The full flexibility characteristic enables the device to work under 300% stretching deformation without degrading performance. Furthermore, the superhydrophobicity and self-cleaning properties provide the TENG additional water energy harvesting ability. Under water flowing rate of 11 mL/s, the output reach approximately to 36 V, and 10 μA. The bifunctional energy harvesting ability, together with good transparency, high stretchability, and robust superhydrophobicity make the TENG a promising sustainable energy source for next-generation electronic devices.

## 1. Introduction

Rapid advancements in nanotechnology effectively accelerate the development of flexible electronic devices ranging from flexible sensors, soft robotics, and roll-up displays to bioinspired artificial skins [1–8]. Meanwhile, the rapid growth of wearable devices put forward higher requirement to the corresponding flexible energy supply units [9–11]. Fundamentally, the power sources should be comparable flexible, shape adaptive, conformally attached to irregular surfaces. Additionally, the robust mechanical durability which can operate under various mechanical deformations, such as folding, crumpling, and stretching without deterioration of their performance is also crucial for practical applications. Compared to traditional rechargeable batteries suffering from heavy weight, bulky volume, and limited lifetime, directly harvesting renewable energy from our living environment and human bodies have been considered a more attractive way to power a variety of portable and wearable electronic devices [12,13]. Recently, flexible energy harvestors that can harvest multiform energy sources including solar, wind, heat, and mechanical vibrations based on various mechanisms have been developed [14–17]. However, due to the intrinsic energy conversion mechanism and the restriction of device configuration, it is hard to achieve full flexibility to be integrated into the flexible systems. Triboelectric nanogenerators (TENGs), based on the coupling effect of triboelectrification and electrostatic induction to convert mechanical energy into electricity, have a wide choice of materials and a simple device configuration, which have potential for high

* Corresponding author. State Key Laboratory for Manufacturing Systems Engineering, Xi'an Jiaotong University, Xi'an, Shaanxi, 710049, China.
** Corresponding author. School of Materials Science and Engineering, Nanyang Technological University, 50 Nanyang Avenue, 639798, Singapore.
*E-mail addresses:* jyshao@mail.xjtu.edu.cn (J. Shao), pslee@ntu.edu.sg (P.S. Lee).

https://doi.org/10.1016/j.nanoen.2019.103904
Received 12 June 2019; Received in revised form 3 July 2019; Accepted 12 July 2019
Available online 17 July 2019

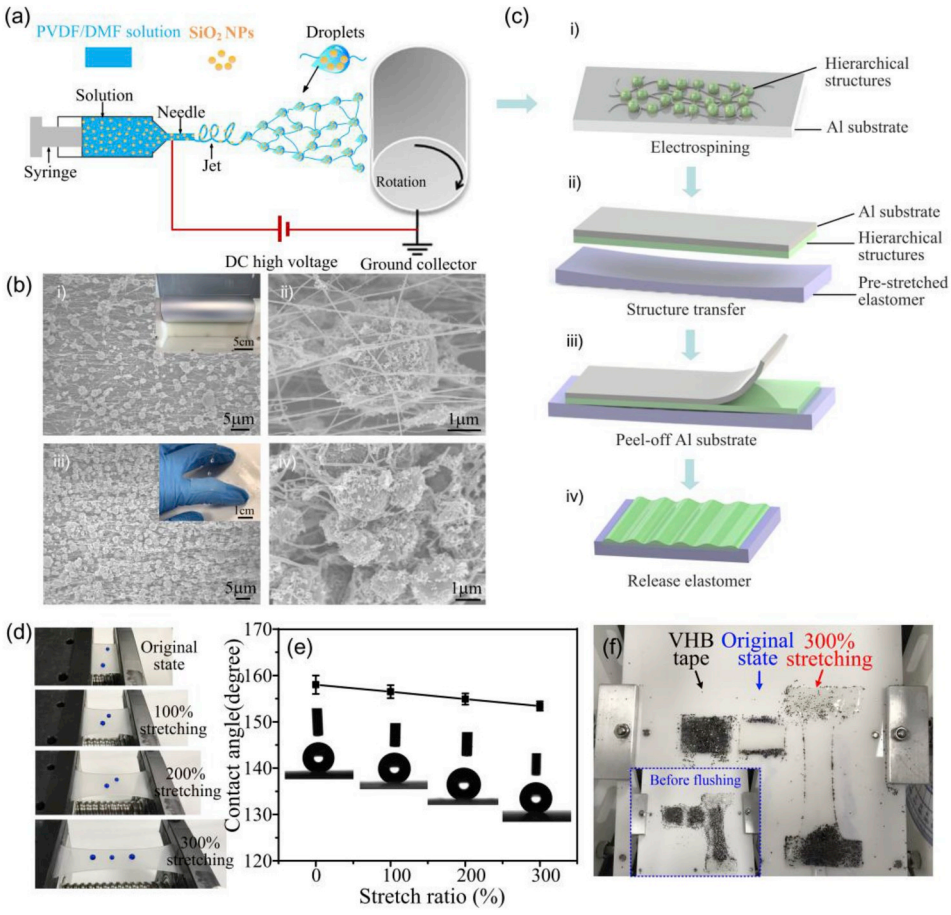


**Fig. 1.** (a) Schematic illustration of electrospinning process to fabricate hierarchical structures. (b) The SEM images of the electrospun hierarchical structures using on Al foil (i,ii) and transferred hierarchical structures on released VHB elastomer (iii,iv). The concentration of the electropsun solution is 50 mg/mL. (c) Experimental methods for transferring the electrospun hierarchical structures onto pre-stretched VHB elastomer. (d,e) The photographs and contact angles of the hierarchical structures under stretching deformation. (f) Self-cleaning performance of pure VHB tape, original TENG device and 300% stretched device.

stretchable applications [18–20]. Especially for triboelectric devices operated under single-electrode mode, they have the advantages of cost-effectiveness, easy fabrication, extremely efficient and can be effectively integrated with wearable devices to harvest irregular mechanical impulses [21–24].

Since the invention of the first triboelectric generator in 2012, growing works are committed to develop high performance TENGs by improving their design, output, stretchability and manufacturability to broaden their breadth of applications [25–29]. For example, the coaxial fiber structure [30],interlocking kirigami structure [31], serpentine shape stainless-steel thread [32,33] are designed to construct stretchable TENGs and show great potential in textile-based energy harvesting applications. However, the Young's modulus mismatch between the used rigid metal electrodes and elastic polymers restrict their stretchability, and cannot provide the maximum freedom under mechanical deformations. To take a step further, various conductive nanomaterials including silver nanowires, carbon nanotubes, carbon black are mixed with silicone rubber to obtain multiple and complicated deformation ability [34–37]. More recently, ionic conductors and liquid electrodes were exploited as extremely stretchable and transparent electrodes used for stretchable TENGs [38–41]. Although there are significant evolutions on the study of stretchable electrodes, the triboelectric layer of the aforementioned devices are mainly flat films. In fact, the surface roughness of the contact surface is critical for improving the output of TENGs [42,43]. Fabricating micro/nanostructures has been demonstrated an effective way to enlarge the friction area and enhance the triboelectric charge density. For example, micro patterns (pillars, cubes, pyramids) [44,45], micro/nano dual-scale patterns [46], nanoscale patterns (dots, lines, holes, and rings) [47–49], inverse-opal structures [50], and fish-scale-like microstructures [28] have been fabricated to construct high output triboelectric devices. However, limited by stretchability, the fabricated micro/nanostructures are hard to be integrated with the stretchable electrodes to fully exert their advantages. It is urgently essential to explore new strategy to fabricate stretchable micro/nanostructures to construct TENGs with high output and stretchability.

Including the mechanical impact, TENG has been demonstrated for harvesting multiform energies such as vibration, wind, and water [51–57]. The water related energy sources in the form of waterfalls, rainwater, and ocean waves provide inexhaustible amounts of energy for realizing the self-powered systems, and therefore has attracted worldwide interests [58–63]. In principle, water energy based TENGs should have superhydrophobic surface to prevent formation of water layer on their surface, as surface triboelectrification would be screened by the existing water layer [64]. So far, various technologies such as photolithographic, nanoimprinting, etching, and subsequent surface modification have been reported to fabricate superhydrophobic surface and construct TENGs [64–67]. These methods either need costly silicon molds to create nanostructures or involve high temperature, high vacuum, or multistep fabrication process, which are not suitable for large scale actual applications. Therefore, it is highly desirable to develop a scalable and low cost strategy to create superhydrophobic structures for practical application. Furthermore, stretchability and transparency property should be considered to be integrated into the water-energy based TENGs for use in flexible raincoat, vehicle glass or even building for harvesting energy from raindrops. Overall, fabricating TENGs with high transparency, strong power generation, and good stretchability, especially with the capability of harvesting multiform energy sources are extremely appealing but still remain highly challenging.

Herein, we report a novel electrospin-transfer strategy to create $SiO_2$/P(VDF-TrFE) hierarchical micro-nanostructures with good transparency, superhydrophobicity and stretchability properties for

effectively harvesting mechanical energy and water energy. The transparent and superhydrophobic $SiO_2$/P(VDF-TrFE) hierarchical structures are directly fabricated by a scalable electrospinning technology, and then reliably transfer to a pre-stretched elastomer to extend stretchability. After assembling with hydrogen slime electrode, the resulted bimodal single-electrode TENG shows a good transparency of 80%, and maintains superhydrophobicity even at 300% stretching deformation. Owing to the high flexibility and large surface area of the hierarchical structures, the $SiO_2$/P(VDF-TrFE) hierarchical structures generate 3 times higher voltage than the pristine $SiO_2$/P(VDF-TrFE) flat film under the same mechanical tapping. In addition, the TENG device shows robust output stability under long-term pressing and extreme stretching deformations up to 300%. Furthermore, the stable superhydrophobic property of the hierarchical structures enables additional water energy harvesting ability. Under continuous water flow, stable electric outputs are generated to power electronic devices, indicating their promising applications in self-powered electronics.

## 2. Results and discussion

### 2.1. Electrospun-transfer hierarchical micro-nanostructures

The schematic of electrospinning process to fabricate $SiO_2$/P(VDF-TrFE) hierarchical micro-nanostructures is illustrated in Fig. 1a. In our strategy, poly(vinylidene difluoride) (PVDF) or its copolymers are selected as the polymer matrix of the nanocomposites for their advantageous properties of flexibility, spinnability, high chemical stability and strong negative triboelectric characteristics [68]. The $SiO_2$ nanoparticles (NPs) have been demonstrated as effective additive nanomaterials for roughening the surface and enhancing charge density in triboelectric devices [69]. Thus, a nanocomposite precursor solution of $SiO_2$/P(VDF-TrFE) is prepared for the electrospinning. Being different from traditional electrospinning process which has been widely used to fabricate align or random nanofibers, [70,71] we utilize the precursor solution with a relative dilute concentration to create hierarchical micro-nanostructures. During the electrospinning process, the solution jet is elongated by strong electric field and solidifies quickly with accompanying evaporation of solvent. Therefore, the concentration of the solution is crucial for the electrospinning morphology for a fixed nozzle-to-collector distance and the applied voltage constant. On this basis, the precursor solutions with three different concentrations (5, 50, 100 mg/mL) were prepared for electrospinning experiments, more descriptions can be seen in the Experimental Section. A high concentration of 100 mg/mL makes the solution jet uniformly elongate and solidify quickly, and forming polymeric nanofibers (Supporting Figs. S1a and b), which in accordance with most electrospinning structures in literatures [72]. When the precursor solution decreases to 50 mg/mL, as the surface tension diminishes quickly, the solution jet is hard to maintain continuous and prefer to shrink to liquid droplets (Fig. 1a). The uniformly distributed liquid droplets finally solidify to hierarchical micro-nanostructures, as shown in Fig. 1b–i. Meanwhile, some polymer solutions solidify to nanofibers and interweave to form a 3D network, further enhancing the surface roughness (Fig. 1b–ii). However, a very low viscosity (5 mg/mL) solution does not have enough materials to sustain the elongation of the solution jet, it ultimately forms nanocomposite film, as shown in Figs. S1c and d. From above results, we use an optimized concentrated solution of 50 mg/mL to electrospin hierarchical micro-nanostructures. Furthermore, in order to fabricate hierarchical structures with superhydrophobic property as well as good transparency, the collecting time is optimized to 40min (Fig. S2). After annealing at 100 °C for 2 h to evaporate solvent and obtain high crystallinity, the electrospun $SiO_2$/P(VDF-TrFE) hierarchical structures are transferred onto a 300% pre-stretched VHB elastomer to extend their stretchability. Fig. 1c illustrates the schematic of transfer process. Due to the good elasticity of the elastomer which leads to a full contact during the transfer process, the electrospun $SiO_2$/P(VDF-TrFE) structures were almost fully transfer to the surface of the elastomer, as shown in Fig. S3. After peeling off the Al substrate and release the elastomer, the transferred $SiO_2$/P(VDF-TrFE) structures are shrunk together to form a higher density structures with good stretchability. Fig. 1b–i, ii show the electrospun $SiO_2$/P(VDF-TrFE) hierarchical structure on Al substrate. The transferred structures on the elastomer are shown in Fig. 1b–iii,iv. The inset of Fig. 1b–i shows the photography of electrospun hierarchical structures on Al foil, which is attached on a rotatable drum. The rotated collection method enables a large area of electrospinning. The right inset picture of Fig. 1b–iii show the transferred structure attached on the joint of the finger, which exhibits good flexibility, transparency and superhydrophobicity. A corresponding demo can be seen in Supporting Video S1. Fig. 1d and e shows the photographs and contact angles of the hierarchical micro-nanostructures at different stretching deformation. Although the contact angles show slightly decreasing trend when the device is under stretching deformation, it still shows superhydrophobicity under 300% stretching condition. Fig. S4 shows the SEM images of structures at different stretching deformation. As the stretching ratios increase, the density of the hierarchical structures are gradually decreasing, which leads to the reduction of the contact angle. Including superhydrophobicity property, self-cleaningproperty is essential to achieve stable performance in harsh environment. Fig. 1f shows the self-cleaning experiment of fabricated devices. A blue dye solution is applied to wash the carbon dust that coated on uncoated elastomer substrate, original device without stretching and a device under 300% stretching deformation. The bottom left inset shows the dust cover on the samples before flushing. After flushing, the dust on our fabricated device was successfully flushed away by the blue dye droplets, exhibiting a good self-cleaning performance for both dust and dye solution. The detail demo can be seen in Video S2. Besides, the good superhydrophobic performance can be maintained even when the device was under dynamic stretching deformation (Video S3). The good flexibility, stable superhydrophobicity and self-cleaning property enable the structure to be applied in harsh environment and be integrated into flexible or wearable systems.

Supplementary video related to this article can be found at https://doi.org/10.1016/j.nanoen.2019.103904.

### 2.2. Construct transparent and stretchable bimodal TENG

In order to fully exploit the advantages of the hierarchical structures, hydrogel slime was used as ionic conductor electrode and integrated with the hierarchical structures to construct transparent and stretchable TENG, as shown in Fig. 2a. In order to create a space to store and seal the hydrogel slime electrode, one layer elastomer with an opening was first attached onto elastomer substrate. Then, the ionic conductor was bladed into the cavity as electrode of TENG. After inserting a thin copper metal wire into the hydrogel slime as conducting wire, the transferred hierarchical structures layer was attached to seal the hydrogen slime electrode. The strong adhesion of the elastomer VHB tape can bond the three layers to form a sealed structure and prevent the hydrogel slime electrode from drying up. Fig. 2b shows the triboelectric mechanism of the TENG operated under solid-solid contact driven mode. According to the triboelectric series, PVDF based hierarchical structures are high electronegative, so when other objects (typically human skin or dielectric materials) are in contact with their surface, charges will transfer from the objects to the hierarchical structures, making the hierarchical structures negatively charged and the objects have the same amount of positive charges (Fig. 2b–i) [73–75]. During the separating of the objects, the negative triboelectric charges on the hierarchical structures layer lead to electrostatic induction on the accumulation of positive ions ($Na^+$) at the hierarchical structures/slime interface and negative ions ($B(OH)^{4-}$) at the slime/metal wire interface, which in turn drive the electrons flow from the metal wire to the ground, generating an electric pulse (Fig. 2b–ii).

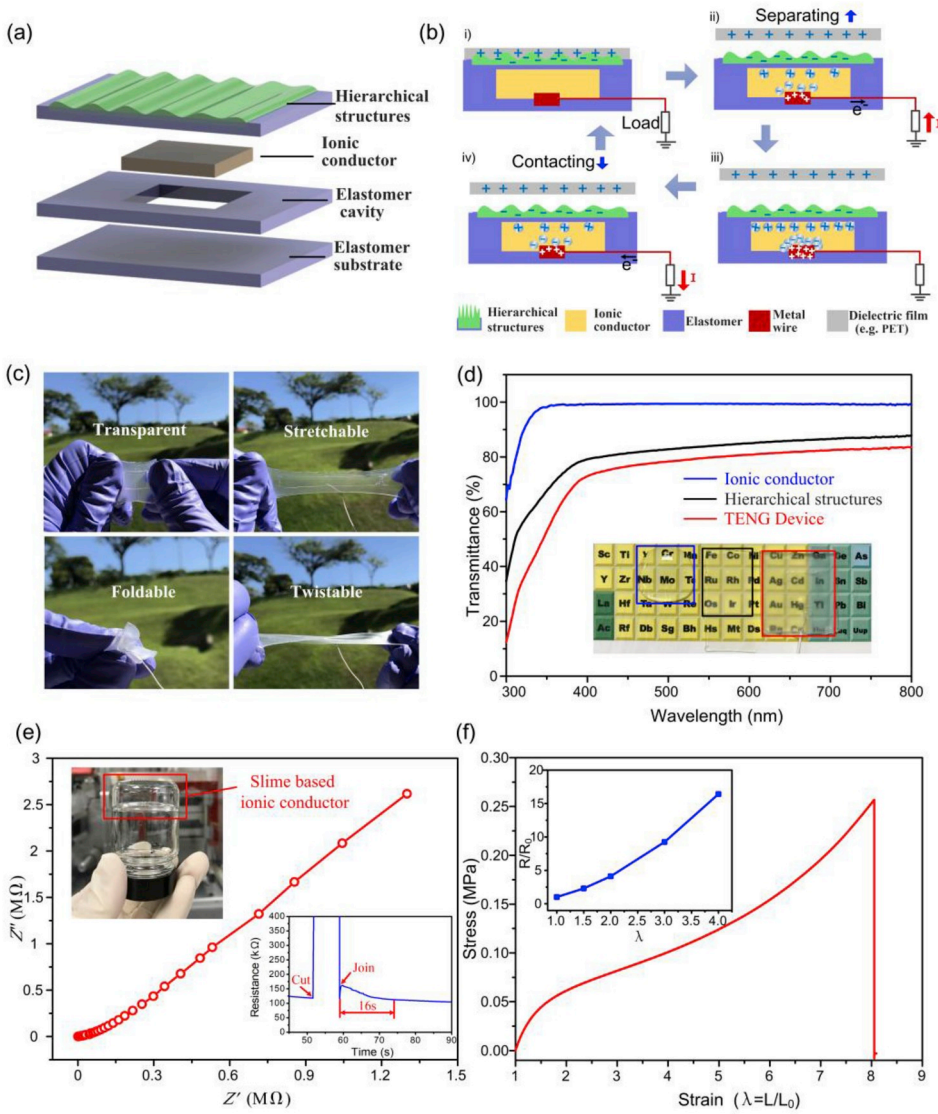


**Fig. 2.** (a) Schematic diagram of the triboelectric nanogenerator. (b) The energy harvesting mechanism of the TENG operated under single electrode mode. (c) The photographs of the resultant TENG device in its original state, stretchable, foldable, and twistable state. (d) The transmittance spectrum of ionic conductor, hierarchical structures, and the resultant TENG device. (e) Electrochemical Impedance Spectroscopy (EIS) measurement on the slime ionic conductor. The ionic conductor was sandwiched between two ITO glass with the dimension: width × length × thickness = 15 mm × 15 mm × 0.5 mm. (f) The stress-strain of the TENG device. Inset show the resistance change of the ionic conductor measured as a function of the stretching strains.

When the object moves far away from the hierarchical structures layer, the TENG reaches electrostatic equilibrium state and no output is generated (Fig. 2b–iii). When the object gets close to the surface, positive charges on the object will decrease the distribution of electric field on slime electrode and drive electrons to flow from ground to the copper electrode (Fig. 2b–iv). Therefore, an alternating electrons flow in the external load will be observed with cycles of contacting and separating process. A fabricated sample is shown in Fig. 2c, which exhibits good transparency and full stretchablility. As shown in the digital photograph in Fig. 2d, the transparency of the ionic conductor, hierarchical structures film, and the triboelectric device are about 99, 83, and 80% at 550 nm, respectively. The conductivity of slime ionic conductor was tested by the electrochemical impedance spectroscopy (Fig. 2e). Because of positive ($Na^+$) and negative ions ($B(OH)^{4-}$) among the slime, the produced slime exhibited a low resistivity of 4140 Ω·cm. The inset shows the self-healing property of the slime conductor. The slime conductor was bifurcated in the center and the two bifurcated parts were electrically sealed and recovered its original resistance among 16s. The mechanical property of the TENGs was tested by uniaxial tensile measurement. As shown in Fig. 2f, the device shows an ultimate stress of 0.26 MPa at a stretch ratio of 8. The inset of Fig. 2e shows the relationship between the resistances of the hydrogel slime and the stretching strains. The resistance change is almost accorded to $R/R_0 = \lambda^2$ with the stretching ratios, λ, indicating that the conductivity of the hydrogel slime is almost independent of the stretching ratios. From above results, self-healing property and the stable conductivity of the hydrogen slime under stretching deformation can ensure stable performance of the resultant TENG device.

### 2.3. Mechanical energy harvesting of the TENG under solid-solid contact driven mode

The energy harvesting performance of the TENG device under the solid-solid triboelectrification was firstly studied by applying mechanical forces to contact and separate the device. In experiment, a PET dielectric film was attached on the vibrator. The commercial PET film was chosen as the dielectric film for their good contact triboelectrification property, good mechanical property and stable chemical property, which ensures stable and longtime output during the measurement. The initial distance between the PET film and hierarchical structures layer of the sample was adjusted to 5 mm. Fig. 3 a,b shows the generated electric outputs at a compressing force of 20 N and 5 Hz. The TENG device generated the approximate output voltage of 170 V, current density of 12.5 μA/cm$^2$, and charge transfer density of 24 nC/cm$^2$ (Fig. S5). For comparison, a control sample of $SiO_2$/P(VDF-TrFE) bulk film was measured. Under the same measurement condition, the control sample shows an output voltage of 56 V, as shown in the inset figure of Fig. 3c. The enhanced electric output can be ascribed to the

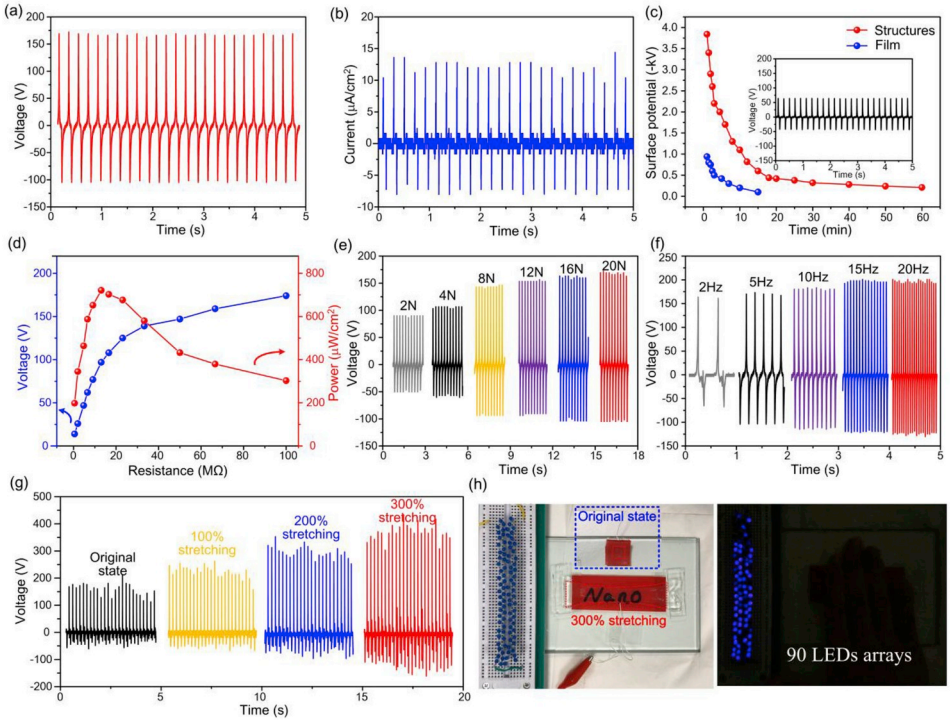


**Fig. 3.** Output characterization of the TENG device under mechanical impacts. (a) Output voltage. (b) Current density. (c) Surface potential. The inset of Fig. 3c shows the output of $SiO_2$/P(VDF-TrFE) bulk film. (d) The effective instantaneous power and output voltages across various loading resistors. (e) The output voltages under different compressive forces with a constant frequency of 5 Hz. (f) Output of the device under a same force of 20 N with different frequencies. (g) Output of the TENG in the original state and under the different stretch ratios by hand touching. (h) The electricity generated from the device under 300% stretching was directly used to light 90 LEDs without any storage units.

increased surface area of electrospun hierarchical structures, which can induced more triboelectric charges during electrification process. Fig. S6 shows the SEM images of the bulk film. Compared with electrospun micro-nano hierarchical structures, the nanocomposite film show relative flat surface and there are only some $SiO_2$ nanoclusters appeared on the surface. Fig. 3c shows surface potential of the hierarchical structures and film sample after 20 times of contact and separate process. The surface potential of the hierarchical structures shows higher initial value and longer retention duration, which are in accordance with the measured triboelectric outputs. The effective instantaneous power of the TENG device was characterized by measuring the voltages across different load resistors. A maximum output power density of 720.5 μW/cm$^2$ was achieved with an external load resistance of 13 MΩ (Fig. 3d). The effect of mechanical force on the performance of the device was investigated by applying force with different magnitudes ranging from 2 to 20 N (Fig. 3e). The output voltages gradually increase initially with the applied force and then remain constant. The output tendency is attributed to the elasticity of the TENG device. High pressure will induce large deformation of the flexible device, thereby increasing the effective contact area and electrostatic charges. When the pressure is high enough to make the PET film fully contact with the device, the output maintains the maximum value. The output performance of the TENG device under different frequencies at constant amplitude of 20 N is shown in Fig. 3f. The device can generate the corresponding outputs along with the increasing of frequency from 2 to 20 Hz, which shows strong ability for harvesting mechanical forces with a variety of frequency and amplitude in our living surroundings. Furthermore, due to the full flexibility of all the components, the TENG device shows stable output performance under 3 h continuous compressing, as shown in Fig. S7. In order to demonstrate the application for harvesting bio-mechanical energy, the fabricated device was touched by human hand on the original state and under different stretching deformation, as shown in Fig. 3g. The output voltages increase with the stretching ratio and reach up to nearly 400 V when the device is at 300% stretching deformation. The enhanced performance can be attributed to dramatically increasing touched area under stretching deformation. When the hierarchical micro-nanostructures based TENG device is stretched, the resistances of the slime ionic conductor have some level of increase. Furthermore, the hierarchical micro-nanostructures on the triboelectric layers will deform, this will decreasing the surface charge density, which will decrease the output performance. On the other hand, the obvious increased touching area of the elastomer film at stretching state will effectively increase the contacting area for the electrification, thus improving the output performance. In the test of Fig. 3g, human hand was almost fully touching the whole area of the TENG device, so the dramatically increasing contact area plays a dominant role in the performance, therefore, the output voltages of the TENG under stretching state keep increasing. The strong power generation performance under stretching deformation enables the TENG device to work under harsh conditions with large deformation. For demonstrating the TENG device in the application of powering commercial electronics, the generated electricity from TENG device under 300% stretching are used to directly lit up a series of 90 blue LEDs (Fig. 3h and Video S4), which would be valuable in realization of self-powered electronics.

Supplementary video related to this article can be found at https://doi.org/10.1016/j.nanoen.2019.103904.

### 2.4. Water energy harvesting of the TENG under the liquid-solid contact driven mode

The hierarchical structures have been demonstrated to effectively enhance the triboelectric output by improving the surface area of the triboelectric layer. Meanwhile, the superhydrophobicity of hierarchical structures endows the TENG an additional ability to harvest water-based energy. The working mechanism of the TENG device under solid-liquid triboelectrification is originated from the contact electrification process when water droplets contact with the hydrophobic structures. The detail working mechanism was described in Fig. S8. To achieve effective triboelectric output, the water droplets should be completely removed from the hydrophobic hierarchical structures after electrification process. In addition to the high contact angle (shown in Fig. 1e.f), the hierarchical structures also show a sliding angle of 6°(Video S5) and a very low shedding angle of 3°(Video S6). The superhydrophobic property can avoid a residual liquid film under flowing water and resulting in the change of contact surface area between water

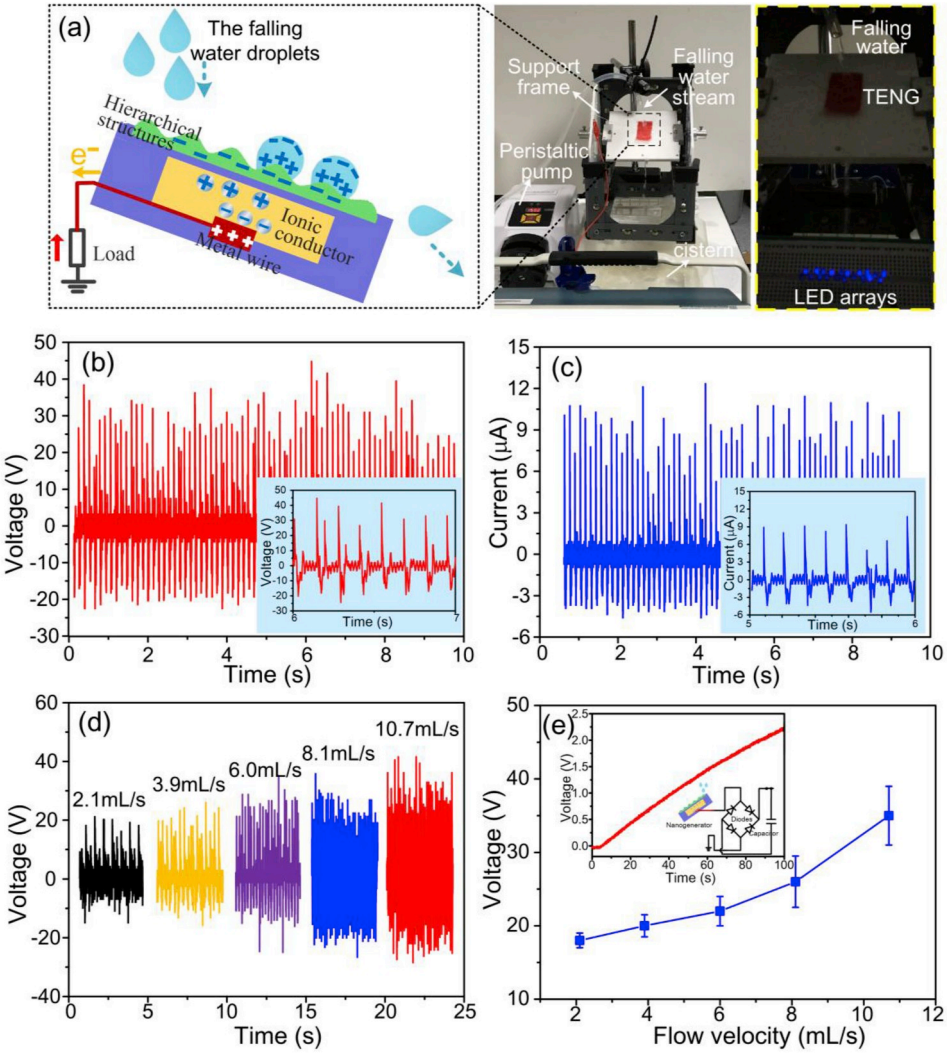


**Fig. 4.** Output characterizations of the TENG device under flowing water. (a) The schematic diagram and experimental setup for water energy harvesting. Continuous output voltage (b) and current (c) under a water flowing of 11 mL/s. (d,e) The relationship between the output voltage and the flow velocity of water. The inset figure shows the voltage across a capacitor during the charging process under water flow.

drop and hierarchical structures, which is essential for electrical power output. To demonstrate the possibility of using the TENG for harvesting water energy, the generated electric output of TENG was measured under flowing water. As shown in Fig. 4a, The TENG device was fixed on a support frame and the water outlet was set above the TENG. The flowing rate of water can be controlled by peristaltic pump. The typical output voltage and current curves generated from TENG are shown in Fig. 4b and c. The output voltage achieves approximately to 36 V, and generated current exceed 10 μA under a flowing rate of 11 mL/s. The inset figure of Fig. 4b and c shows the enlarge measured waveform. The fluctuation of the electric outputs was caused by the irregular amount of water in contact on the hierarchical structures that is constantly changing during the water flowing process. When the superhydrophobic hierarchical structures were replaced with a flat film, there was a noticeable decrease in output (Fig. S9). The insufficient hydrophobicity of the flat film will cause some water drops to remain on the sample surface, results in a lower and less frequent output compared with hierarchical structures, demonstrating the significant contribution of the superhydrophobic surface. The high output electricity can be used to directly power 20 LEDs in series, as shown in the right inset of Fig. 4a (Video S7). Furthermore, the output voltages under different flow velocity were measured, as shown in Fig. 4d and e. The increased velocity of the flow water will accelerate the process of the water droplets contacting and leaving the hierarchical structures, which leads to faster charge transfer in the circuit. The positive relationship between the output voltages and flow velocity of falling water may provide a self-powered sensing solution for measuring the flow velocity. The generated electricity under water flow can also be used to charge commercial capacitor, as shown in the inset of Fig. 4e. Under a falling water velocity of 10.7 mL/s, it takes about 100 s to charge a capacitor of 10 μF up to 2.2 V, which shows a fast charging ability. The strong power generation and sensing performance under water flow enables the TENG device wide promising applications for water energy harvesting.

Supplementary video related to this article can be found at https://doi.org/10.1016/j.nanoen.2019.103904.

## 3. Conclusion

A transparent and stretchable bimodal TENG with superhydrophobic and self-cleaning ability is proposed and demonstrated for applications in harvesting mechanical energy and water energy. The core hierarchical micro/nanostructures were directly fabricated by a facile and scalable electrospin-transfer method. It is found that the surface tension of precursor solution plays an important role in the creation of hierarchical structures. After integrating with slime-based ionic conductor, the resultant TENG shows a high transparency of 80%,

mechanical transformability with stretchable, foldable, and twistable properties, and maintains superhydrophobic even at 300% stretching deformation. Owing to the enhanced surface area, the hierarchical structures generate an output voltage 3 times higher than that of flat film under the same mechanical force during tapping. The strong charge generation property of the hierarchical structures was further verified by the surface potential measurement. In addition, the fabricated TENG showed high durability against large stretching deformation up to 300% strain and sustained its output under cycling test with duration of 3 h, indicating its applicability under extreme deformation conditions. Moreover, by virtue of the superhydrophobic property, the TENG was successfully demonstrated for water energy harvesting. Under the impact of a water stream at a flowing rate of 11 mL/s, the generated voltage and current can reach 36V and 10 μA, respectively, which successfully driving LED arrays and charging commercial capacitors, demonstrating its applicability to power electronic device. Because of the distinctive features of good transmittance, highly flexibility, stretchability, strong power generation, and the ability to harvest multi-energy sources, the proposed TENG will have a wide potential application on self-powered electronics.

## 4. Methods

### 4.1. Preparation of electrospun precursor solution

$SiO_2$ nanopowders (NPs) with an average diameter of 10–20 nm were first mixed with DMF and ultrasonic stirred for 5 h to prevent agglomeration. P(VDF-TrFE) powders were then added to produce solutions with a predefined 30 wt% of $SiO_2$ NPs with respect to P(VDF-TrFE) by stirring for 2 h in a heated water bath at a temperature of 60° to obtain a uniform solution. The precursor solutions with three different concentrations (5, 50, 100 mg/mL) were prepared for electrospinning experiments to find an optimized mixing ratio. About 6 mL of the precursor solution was placed in a 10 mL syringe equipped with a blunt metal needle. The solution feed rate was adjusted to 0.5 mL/h by syringe pump. A stainless steel roller covered with aluminum foil was employed as the collector. The rotational speed was set at 1500 rpm. The distance between the needle tip and collector was about 10 cm, and the voltage was set at 18 kV. The VHB tape with a thickness of 250 μm (VHB 4010, 3 M, USA) was used as the elastomer substrate. For a fair comparison of the triboelectric performances of hierarchial structure layer with a sample of $SiO_2$/P(VDF-TrFE) bulk film, the solution with a concentration of 50 mg/mL was spin-coated into film and annealing at 100 °C for 2 h to evaporate solvent.

### 4.2. Fabrication of hydrogen bonded slime hydrogel electrode

Following our previous report, [76] the PVA powders were slowly dissolved in deionized (DI) water as a concentration of 10 wt% while stirred vigorously at a temperature of 90 °C to obtain uniform and clear solution. The solution was subsequently mixed with 4 wt% borax in DI solution in a volume ratio of 4:1, while vigorously stirring with a spatula until the mixture was complete gelled to form the transparent and viscous hydrogen bonded slime.

### 4.3. Measurement and characterizations

The morphologies of the electrospun structures were characterized using a field-emission scanning electron microscope (FE-SEM, 6340). The optical transmittance was measured by a Shimadzu UV-3600 spectrophotometer equipped with an optical integration sphere. The contact angle was measured by contact angle measuring system (Dataphysics OCA15 Pro) with droplets of 5 μL. The surface potential values were measured by an Electrostatic Voltmeter (Trek, Model 542 A). During the measurement of the surface potential, the sample was placed onto a conductive substrate, which was ground connection to avoid the distractions. The probe of Electrostatic Voltmeter was placed on the top of the sample surface about 2–3 mm, which is near enough to detect a stable surface potential. Then the value of the surface potential can be directly read from the display screen of the Electrostatic Voltmeter. The performance of the TENGs was evaluated by analyzing the output signals measured by a customized system, which was mainly composed of a function generator (Agilent 33220A), electromechanical vibrator (SINOCERA JZK-10), and power amplifier (SINOCERA YE5871A). The magnitude of applying force was measured by a force transducer (SINOCERA CL-YD-331). An oscilloscope (Tektronix DPO3034) with a probe of 100 MΩ is used to measure the output voltage. Short-circuit current from the device is measured using a low-noise current preamplifier (SR570, Stanford Research Systems). The transferred charge was measured using a Keithley 6517B system electrometer.

## Competing financial interests

The authors declare no competing interests.

## Acknowledgments

This work was supported by the National Natural Science Foundation of China (Grant Nos. 91323303, 51421004, 51522508), National Postdoctoral Program for Innovative Talents (No. BX20180251), China Postdoctoral Science Foundation (No. 2019M653588) and Natural Science Basic Research Plan in Shaanxi Province of China (No. 2018JQ5128). This work was also supported by the NRF Investigatorship award no. NRF-NRFI2016-05, and the Campus for Research Excellence and Technological Enterprise (CREATE) that is supported by the National Research Foundation, Prime Minister's Office, Singapore.

## Appendix A. Supplementary data

Supplementary data to this article can be found online at https://doi.org/10.1016/j.nanoen.2019.103904.

## References

[1] W. Wu, L. Wang, Y. Li, F. Zhang, L. Lin, S. Niu, D. Chenet, X. Zhang, Y. Hao, T.F. Heinz, J. Hone, Z.L. Wang, Nature 514 (2014) 470–474.
[2] Y. Duan, Y. Huang, Z. Yin, N. Bu, W. Dong, Nanoscale 6 (2014) 3289–3295.
[3] Y. Huang, N. Bu, Y. Duan, Y. Pan, H. Liu, Z. Yin, Y. Xiong, Nanoscale 5 (2013) 12007–12017.
[4] L. Hines, K. Petersen, G.Z. Lum, M. Sitti, Adv. Mater. 29 (2017) 1603483.
[5] J. Kim, M. Lee, H.J. Shim, R. Ghaffari, H.R. Cho, D. Son, Y.H. Jung, M. Soh, C. Choi, S. Jung, K. Chu, D. Jeon, S.T. Lee, J.H. Kim, S.H. Choi, T. Hyeon, D.H. Kim, Nat. Commun. 5 (2014) 5747.
[6] J. Wang, C. Yan, G. Cai, M. Cui, A. Lee-Sie Eh, P. See Lee, Adv. Mater. 28 (2016) 4490–4496.
[7] J. Shao, X. Chen, X. Li, H. Tian, C. Wang, B. Lu, Sci. China Technol. Sci. (2019) 1–24.
[8] X. Chen, J. Shao, N. An, X. Li, H. Tian, C. Xu, Y. Ding, J. Mater. Chem. C 3 (2015) 11806–11814.
[9] A. Proto, M. Penhaker, S. Conforto, M. Schmid, Trends Biotechnol. 35 (2017) 610–624.
[10] X. Chen, X. Li, J. Shao, N. An, H. Tian, C. Wang, T. Han, L. Wang, B. Lu, Small 13 (2017) 1604245.
[11] X. Chen, H. Tian, X. Li, J. Shao, Y. Ding, N. An, Y. Zhou, Nanoscale 7 (2015) 11536–11544.
[12] F.R. Fan, W. Tang, Z.L. Wang, Adv. Mater. 28 (2016) 4283–4305.
[13] J. Xiong, P. Cui, X. Chen, J. Wang, K. Parida, M.-F. Lin, P.S. Lee, Nat. Commun. 9 (2018) 4280.
[14] Y. Liu, N. Sun, J. Liu, Z. Wen, X. Sun, S.T. Lee, B. Sun, ACS Nano 12 (2018) 2893–2899.
[15] H. Wu, Y. Huang, F. Xu, Y. Duan, Z. Yin, Adv. Mater. 28 (2016) 9881–9919.
[16] L. Zheng, G. Cheng, J. Chen, L. Lin, J. Wang, Y. Liu, H. Li, Z.L. Wang, Adv. Energy Mater. 5 (2015) 1501152.
[17] X. Cheng, L. Miao, Y. Song, Z. Su, H. Chen, X. Chen, J. Zhang, H. Zhang, Nano Energy 38 (2017) 438–446.

[18] K. Zhang, Z.L. Wang, Y. Yang, ACS Nano 10 (2016) 4728–4734.
[19] X. He, Y. Zi, H. Guo, H. Zheng, Y. Xi, C. Wu, J. Wang, W. Zhang, C. Lu, Z.L. Wang, Adv. Funct. Mater. 27 (2017) 1604378.
[20] J. Wang, C. Wu, Y. Dai, Z. Zhao, A. Wang, T. Zhang, Z.L. Wang, Nat. Commun. 8 (2017) 88.
[21] S.L. Zhang, Y.-C. Lai, X. He, R. Liu, Y. Zi, Z.L. Wang, Adv. Funct. Mater. 27 (2017) 1606695.
[22] T. Li, J. Zou, F. Xing, M. Zhang, X. Cao, N. Wang, Z.L. Wang, ACS Nano 11 (2017) 3950–3956.
[23] X. Chen, Y. Song, Z. Su, H. Chen, X. Cheng, J. Zhang, M. Han, H. Zhang, Nano Energy 38 (2017) 43–50.
[24] X. Chen, K. Parida, J. Wang, J. Xiong, M.F. Lin, J. Shao, P.S. Lee, ACS Appl. Mater. Interfaces 9 (2017) 42200–42209.
[25] Y. Bao, R. Wang, Y. Lu, W. Wu, Apl. Mater. 5 (2017) 074109.
[26] Z.L. Wang, W. Wu, Angew Chem. Int. Ed. Engl. 51 (2012) 11700–11721.
[27] R. Wang, S. Gao, Z. Yang, Y. Li, W. Chen, B. Wu, W. Wu, Adv. Mater. 30 (2018).
[28] X. Li, C. Xu, C. Wang, J. Shao, X. Chen, C. Wang, H. Tian, Y. Wang, Q. Yang, L. Wang, B. Lu, Nano Energy 40 (2017) 646–654.
[29] Y. Yu, X. Wang, Extreme Mech. Lett. 9 (2016) 514–530.
[30] K.N. Kim, J. Chun, J.W. Kim, K.Y. Lee, J.-U. Park, S.-W. Kim, Z.L. Wang, J.M. Baik, ACS Nano 9 (2015) 6394–6400.
[31] C. Wu, X. Wang, L. Lin, H. Guo, Z.L. Wang, ACS Nano 10 (2016) 4652–4659.
[32] Y.-C. Lai, J. Deng, S.L. Zhang, S. Niu, H. Guo, Z.L. Wang, Adv. Funct. Mater. 27 (2017) 1604462.
[33] P.K. Yang, L. Lin, F. Yi, X. Li, K.C. Pradel, Y. Zi, C.I. Wu, J.H. He, Y. Zhang, Z.L. Wang, Adv. Mater. 27 (2015) 3817–3824.
[34] F. Yi, J. Wang, X. Wang, S. Niu, S. Li, Q. Liao, Y. Xu, Z. You, Y. Zhang, Z.L. Wang, ACS Nano 10 (2016) 6519–6525.
[35] Y.C. Lai, J. Deng, S. Niu, W. Peng, C. Wu, R. Liu, Z. Wen, Z.L. Wang, Adv. Mater. 28 (2016) 10024–10032.
[36] S. Park, H. Kim, M. Vosgueritchian, S. Cheon, H. Kim, J.H. Koo, T.R. Kim, S. Lee, G. Schwartz, H. Chang, Z. Bao, Adv. Mater. 26 (2014) 7324–7332.
[37] S. Li, J. Wang, W. Peng, L. Lin, Y. Zi, S. Wang, G. Zhang, Z.L. Wang, Adv. Energy Mater. 7 (2017) 1602832.
[38] K. Parida, V. Kumar, W. Jiangxin, V. Bhavanasi, R. Bendi, P.S. Lee, Adv. Mater. 29 (2017).
[39] X. Pu, M. Liu, X. Chen, J. Sun, C. Du, Y. Zhang, J. Zhai, W. Hu, Z.L. Wang, Sci. Adv. 3 (2017) e1700015.
[40] J.W. Lee, H.J. Cho, J. Chun, K.N. Kim, S. Kim, C.W. Ahn, I.W. Kim, J.-Y. Kim, S.-W. Kim, C. Yang, Sci. Adv. 3 (2017) e1602902.
[41] K. Parida, J. Xiong, X. Zhou, P.S. Lee, Nano Energy 59 (2019) 237–257.
[42] S. Jin, Y. Wang, M. Motlag, S. Gao, J. Xu, Q. Nian, W. Wu, G.J. Cheng, Adv. Mater. 30 (2018).
[43] Y. Huang, Y. Ding, J. Bian, Y. Su, J. Zhou, Y. Duan, Z. Yin, Nano Energy 40 (2017) 432–439.
[44] F.R. Fan, L. Lin, G. Zhu, W. Wu, R. Zhang, Z.L. Wang, Nano Lett. 12 (2012) 3109–3114.
[45] H.S. Wang, C.K. Jeong, M.-H. Seo, D.J. Joe, J.H. Han, J.-B. Yoon, K.J. Lee, Nano Energy 35 (2017) 415–423.
[46] X.-S. Zhang, M.-D. Han, R.-X. Wang, B. Meng, F.-Y. Zhu, X.-M. Sun, W. Hu, W. Wang, Z.-H. Li, H.-X. Zhang, Nano Energy 4 (2014) 123–131.
[47] L. Zhang, L. Cheng, S. Bai, C. Su, X. Chen, Y. Qin, Nanoscale 7 (2015) 1285–1289.
[48] J. Chun, J.W. Kim, W.-s. Jung, C.-Y. Kang, S.-W. Kim, Z.L. Wang, J.M. Baik, Energy Environ. Sci. 8 (2015) 3006–3012.
[49] Y.S. Choi, Q. Jing, A. Datta, C. Boughey, S. Kar-Narayan, Energy Environ. Sci. 10 (2018) 2180–2189.
[50] K.Y. Lee, J. Chun, J.H. Lee, K.N. Kim, N.R. Kang, J.Y. Kim, M.H. Kim, K.S. Shin, M.K. Gupta, J.M. Baik, S.W. Kim, Adv. Mater. 26 (2014) 5037–5042.
[51] H. Guo, X. Pu, J. Chen, Y. Meng, M.-H. Yeh, G. Liu, Q. Tang, B. Chen, D. Liu, S. Qi, C. Wu, C. Hu, J. Wang, Z.L. Wang, Sci. Robot. 3 (2018) 2516.
[52] Q. Liang, X. Yan, X. Liao, Y. Zhang, Nano Energy 25 (2016) 18–25.
[53] B. Zhang, L. Zhang, W. Deng, L. Jin, F. Chun, H. Pan, B. Gu, H. Zhang, Z. Lv, W. Yang, Z.L. Wang, ACS Nano 11 (2017) 7440–7446.
[54] L. Feng, G. Liu, H. Guo, Q. Tang, X. Pu, J. Chen, X. Wang, Y. Xi, C. Hu, Nano Energy 47 (2018) 217–223.
[55] J. Chen, H. Guo, X. Pu, X. Wang, Y. Xi, C. Hu, Nano Energy 50 (2018) 536–543.
[56] W. Liu, Z. Wang, G. Wang, G. Liu, J. Chen, X. Pu, Y. Xi, X. Wang, H. Guo, C. Hu, Nat. Commun. 10 (2019) 1426.
[57] J. Chen, X. Pu, H. Guo, Q. Tang, L. Feng, X. Wang, C. Hu, Nano Energy 43 (2018) 253–258.
[58] X.J. Zhao, S.Y. Kuang, Z.L. Wang, G. Zhu, ACS Nano 12 (2018) 4280–4285.
[59] X. Li, J. Tao, X. Wang, J. Zhu, C. Pan, Z.L. Wang, Adv. Energy Mater. 8 (2018) 1800705.
[60] J. Xiong, M.-F. Lin, J. Wang, S.L. Gaw, K. Parida, P.S. Lee, Adv. Energy Mater. 7 (2017) 1701243.
[61] Z.L. Wang, T. Jiang, L. Xu, Nano Energy 39 (2017) 9–23.
[62] Q. Zhang, Q. Liang, Q. Liao, F. Yi, X. Zheng, M. Ma, F. Gao, Y. Zhang, Adv. Mater. 29 (2017).
[63] G. Liu, H. Guo, S. Xu, C. Hu, Z.L. Wang, Adv. Energy Mater. (2019) 1900801.
[64] Z.H. Lin, G. Cheng, S. Lee, K.C. Pradel, Z.L. Wang, Adv. Mater. 26 (2014) 4690–4696.
[65] J. Ha, J. Chung, S. Kim, J.H. Kim, S. Shin, J.Y. Park, S. Lee, J.-B. Kim, Nano Energy 36 (2017) 126–133.
[66] J. Chen, H. Guo, J. Zheng, Y. Huang, G. Liu, C. Hu, Z.L. Wang, ACS Nano 10 (2016) 8104–8112.
[67] Y. Su, X. Wen, G. Zhu, J. Yang, J. Chen, P. Bai, Z. Wu, Y. Jiang, Z. Lin Wang, Nano Energy 9 (2014) 186–195.
[68] M.-F. Lin, K. Parida, X. Cheng, P.S. Lee, Adv. Mater. Technol. 2 (2017) 1600186.
[69] T. Huang, H. Yu, H. Wang, Q. Zhang, M. Zhu, J. Phys. Chem. C 120 (2016) 26600–26608.
[70] Y. Huang, N. Bu, Y. Duan, Y. Pan, H. Liu, Z. Yin, Y. Xiong, Nanoscale 5 (2013) 12007–12017.
[71] J. Xiong, H. Luo, D. Gao, X. Zhou, P. Cui, G. Thangavel, K. Parida, P.S. Lee, Nano Energy 61 (2019) 584–593.
[72] Q. Liu, J.H. Zhu, L.W. Zhang, Y.J. Qiu, Renew. Sust. Energ. Rev. 81 (2018) 1825–1858.
[73] H. Zou, Y. Zhang, L. Guo, P. Wang, X. He, G. Dai, H. Zheng, C. Chen, A.C. Wang, C. Xu, Nat. Commun. 10 (2019) 1427.
[74] M. Kanik, M.G. Say, B. Daglar, A.F. Yavuz, M.H. Dolas, M.M. El-Ashry, M. Bayindir, Adv. Mater. 27 (2015) 2367–2376.
[75] Z.L. Wang, ACS Nano 7 (2013) 9533–9557.
[76] G. Cai, J. Wang, K. Qian, J. Chen, S. Li, P.S. Lee, Adv. Sci. 4 (2017) 1600190.

**Dr. Xiaoliang Chen** received his Ph.D. degree from Xi'an Jiaotong University, Xi'an, China, in 2018. He is currently an assistant professor at the State Key Laboratory for Manufacturing Systems Engineering, Xi'an Jiaotong University. His research work is focused on micro/nano manufacturing technologies, flexible sensors, self-powered devices and renewable energy harvesting. He received the grant National Postdoctoral Program for Innovative Talents in 2018.

**Dr. Jiaqing Xiong** received his master's degree from Biomedical Engineering at Chongqing University of Technology in 2012. Receiving his Ph.D. degree from Soochow University in Textile Engineering in 2015. Now he is a research fellow in School of Materials Science and Engineering (Prof. Pooi See Lee's group) at Nanyang Technological University. His research focuses on nanocellulose, transparent conductors, self-powered electronics, flexible and wearable devices, water energy and environmental management.

**Dr. Kaushik Parida** received his master's degree from the School of Metallurgical Engineering and Materials Science of Indian Institute of Technology Bombay, India in 2013.He received his Ph.D. under the supervision of Prof. Pooi See Lee at the School of Materials Science and Engineering in Nanyang Technological University, Singapore. He is current a Research Fellow at Nanyang Technological University. His research focuses on deformable electronics, piezoelectric and triboelectric energy harvester.

**Dr. Meiling Guo** received her Ph.D. degree from School of Mechanical Engineering in Xi'an Jiaotong University, Xi'an, China, in 2016. She is currently a lecturer at School of Mechanical and Precision Instrument Engineering, Xi'an University of Technology, Xi'an, China. Her current research focuses on nano-surface manufacture and science, nanotribology and triboelectric nanogenerator.

**Cheng Wang** received his B.S. degree from Xi'an University of Technology, Shaanxi, China, in 2017. He is currently working toward the M.S. degree at Xi'an University of Technology. His current research interests focus on micro-nano manufacturing technologies, triboelectric energy harvester and self-powered devices.

**Chao Wang** received his B.S. degree from Jilin University, Chang Chun, China, in 2014. He is currently working toward the Ph.D. degree at the State Key Laboratory of Manufacturing Systems Engineering, Xi'an Jiaotong University, Xi'an, China. His current research interests focus on micro-nano manufacturing technologies for energy harvesting and self-powered sensors.

**Dr. Xiangming Li** received the Ph.D. degree from Xi'an Jiaotong University, Xi'an, China, in 2014. He is currently an associate professor at the State Key Laboratory for Manufacturing Systems Engineering, Xi'an Jiaotong University. He has published more than 40 peer-reviewed research papers. His research interests include energy storage materials and devices, flexible electronics and systems, micro/nano manufacturing technologies, nanosensors and devices. He received the silver prize of HIWIN Doctoral Dissertation Award.

**Prof. Jinyou Shao** received the Ph.D. degree from Xi'an Jiaotong University, Xi'an, China, in 2009. He is currently a Professor at the State Key Laboratory for Manufacturing Systems Engineering, Xi'an Jiaotong University. His research interests include micro/nanomanufacturing techniques, flexible electronics and systems, nanosensors and devices. Prof. Shao received the First Prize Technology Invention Award of the Ministry of Education of China in 2015. He is awarded Changjiang Scholars-Young Category, NSFC Fund for Excellent Young Scholars, New Century Excellent Talents by MoE of China, Shaanxi Young Talents in Science and Technology, ACS Membership Award, etc.

**Prof. Pooi See Lee** received her Ph.D. from the National University of Singapore in 2002. She joined Chartered Semiconductor Manufacturing Ltd (now Global foundries) in research and technology development department upon graduation. She was a recipient of the Norman Hackermann Young Author Award, by ECS, US, in 2001. She joined the School of Materials Science and Engineering, Nanyang Technological University as an Assistant Professor in 2004. She was promoted to tenured Associate Professor in 2009 and full Professor in 2015. Her research focuses on nanomaterials for energy and electronics applications, flexible and stretchable devices, electrochemical inspired devices, and human-machine interface. She received the National Research Foundation Investigatorship, the Nanyang Research Excellence Award in 2016, and the Nanyang Entrepreneurship and Innovation Award in 2017.